Measuring Micro-amp Inductor Currents in Switched-inductor DC–DC Power Supplies

Andrés A. Blanco, *Graduate Student Member, IEEE*, and Gabriel A. Rincón-Mora, *Fellow, IEEE*
Georgia Institute of Technology, Atlanta, Georgia 30332 U.S.A.
E-mail: ablanco@gatech.edu and Rincon-Mora@gatech.edu

***Abstract*—Wireless microsystems can add performance-enhancing, energy-saving, and networked intelligence to inaccessible places like the human body and large infrastructures like factories, hospitals, and farms. For this, they require an onboard source and a power-conditioning circuit that supply microwatts about a prescribed dc voltage. And since tiny dc batteries store little energy, switched-inductor dc–dc converters are popular in this respect, because they dissipate less power than linear regulators and are more accurate than switched capacitors. To monitor how they operate and ultimately meet these expectations, engineers monitor the current flowing through the inductor. In the case of miniaturized supplies, however, inductors switch at 100 kHz – 1 MHz to produce micro-amp currents that are difficult to sense. Although series resistors and magnetically coupled probes are normally viable options, the series components they introduce into the conduction path alter the currents being measured and noise energy obscures the results. But as experimental measurements further show, characterizing and extracting current from the terminal voltages of the inductor is less obtrusive and less sensitive to noise.**

Keywords—Switched inductor, switching dc–dc converter, current measurement, microsupply, microsystem, microwatt.

I. Supplying Microsystems

Wireless microsystems in inaccessible places like the human body and large infrastructures like factories, hospitals, and farms can monitor, process, and transmit information that can save lives and energy and, generally, improve performance [1–2]. Since the sensors, analog–digital (A/D) converters, digital-signal processors (DSP), and transmitters they incorporate from Fig. 1 demand power to operate, these tiny contraptions also include energy sources and power-supply circuits. The latter are usually switched inductors because small batteries cannot afford to lose the power that linear regulators consume and analog functions cannot survive the ripples that switched on-chip capacitors produce [3].

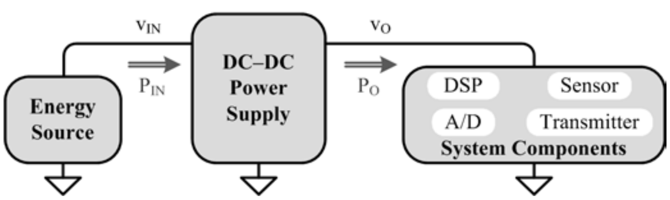

Fig. 1. Typical wireless microsystem.

Interestingly, inductor current i_L dictates several key performance parameters in switching dc–dc converters [4–7]. For one, i_L defines how much power the system draws from the input v_{IN} as P_{IN} and outputs to v_O as P_O. i_L also determines the power that components in the conduction path consume. Plus, i_L's waveform establishes the ripple voltage that appears across the load in v_O. This is why monitoring i_L is critical when evaluating switched-inductor supplies [8–10].

Unfortunately, current levels in miniaturized systems are so low at micro-amps that discerning them in the presence of switching and thermal noise is challenging. And inserting current sensors introduce voltage drops that alter how these currents behave. For more details on this, Section II describes the operation of switched-inductor supplies and the effects of series resistances on i_L. Afterwards, Sections III – V evaluate to what extent magnetically coupled probes, series resistors, and current extractors can reconstruct i_L. Sections VI and VII then compare results and draw relevant conclusions.

II. Switched-inductor Microsupplies

A. Operation

Switched-inductor dc–dc supplies draw and supply energy from the input v_{IN} to the output v_O in alternate cycles of a switching period t_{SW}. For this, switches S_I and S_E in Fig. 2 close to energize inductor L_X from v_{IN}. With a constant positive energizing voltage v_E, L_X's voltage v_L or $L_X di_L/dt$ is constant and i_L in Fig. 3 rises and peaks to $i_{L(PK)}$ at the end of energizing time t_E. S_I and S_E then open and S_D and S_O engage to impress a constant negative voltage v_D across L_X that drains L_X into v_O. i_L, as a result, falls from $i_{L(PK)}$ until L_X depletes after t_D. At this point, when i_L is zero, the system opens S_O and repeats the sequence at the onset of the next switching cycle.

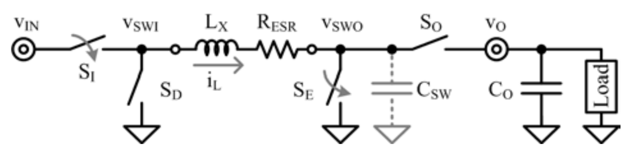

Fig. 2. Switched-inductor dc–dc converter.

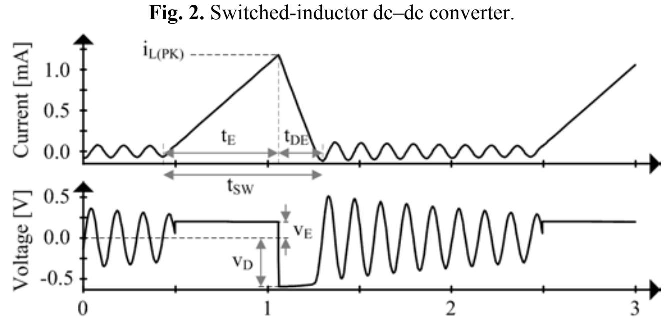

Fig. 3. Measured inductor current and voltage across time.

Power levels are so low in microsystems that $i_{L(PK)}$ is usually not high enough to keep L_X conducting across all of t_{SW}. Notwithstanding, since the parasitic capacitance C_{SW} at the switching node v_{SWO} near v_O is close to v_O after S_O opens, C_{SW} stores charge that L_X draws and returns to C_{SW} to produce the oscillations in Fig. 3. These oscillations fade with time because parasitic resistance gradually dissipates the energy.

The physical size of L_X in miniaturized systems is so low that reasonable inductances include Ohms of equivalent series resistance R_{ESR}. This means v_E and v_D appear across both L_X and R_{ESR}, so the voltage across the inductance is not constant:

$$v_L = L_X\left(\frac{di_L}{dt}\right) + i_L R_{ESR} . \qquad (1)$$

In other words, i_L is not perfectly linear:

$$i_L = \left(\frac{v_L}{R_{ESR}}\right)\left[1 - e^{-\left(\frac{R_{ESR}}{L_X}\right)t}\right] \approx \left(\frac{v_L}{R_{ESR}}\right)t . \qquad (2)$$

Still, v_L is usually in volts and R_{ESR}'s v_{ESR} in millivolts, so i_L is nearly linear. Incidentally, S_O can remain closed when v_{IN} is always higher than v_O because v_L is positive from v_{IN} to v_O and negative from ground to v_O. Similarly, S_I can remain closed when v_O is always greater than v_{IN} because v_L is positive from v_{IN} to ground and negative from v_{IN} to v_O.

B. Measuring Inductor Current

A fundamental challenge when measuring i_L in microsystems is discerning micro-amps from noise i_N at 100 kHz – 1 MHz. In other words, signal-to-noise ratio SNR can be low:

$$\text{SNR} \equiv \frac{i_L}{i_N} . \qquad (3)$$

Another difficulty is that inserting a series resistance R_S distorts i_L, which means the measurement can alter i_L:

$$i_L' = \left(\frac{v_L}{R_{ESR} + R_S}\right)\left[1 - e^{-\left(\frac{R_{ESR}+R_S}{L_X}\right)t}\right], \qquad (4)$$

and produce an error i_E in Fig. 4 that rises with R_S:

$$i_E = i_L - i_L' . \qquad (5)$$

When R_S is so high that R_S's voltage v_S overwhelms v_L, i_L' stops rippling and reduces to v_L/R_S, at which point the error i_E/i_L is 100%. Before that, though, when L_X, R_{ESR}, and R_S are 100 µH, 10.5 Ω, and 19.1 Ω, the error is 5% after 0.55 µs.

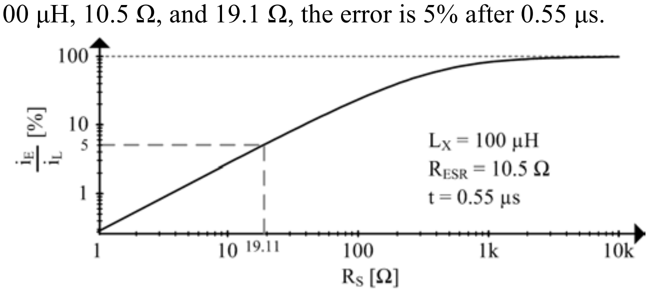

Fig. 4. Measured inductor-current error across series resistances.

III. Magnetically Coupled Probe

One way to measure high-speed currents with micro-amp resolution is to use a magnetically coupled probe like Fig. 5 illustrates. This way, i_L flows through the primary coil L_P and current variations Δi_L couple to the secondary coil L_S. L_S therefore produces a voltage across L_S's parallel resistance R_P that is proportional to Δi_L and the probe's turns ratio N_S/N_P. So, amplifying this voltage with A_V and dividing the result by R_S reconstructs Δi_L in i_S, as Fig. 6 shows.

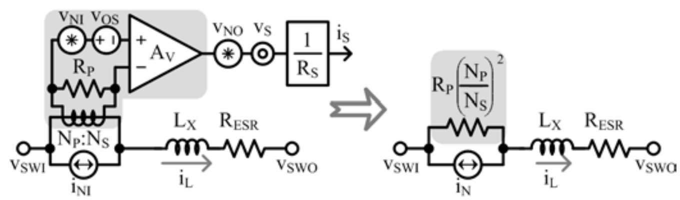

Fig. 5. Magnetically coupled probe network and equivalent primary circuit.

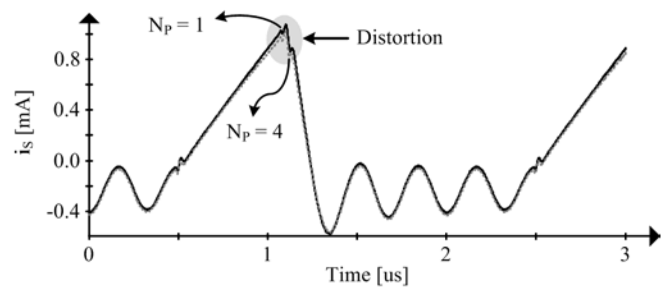

Fig. 6. Measured coupled waveforms with one and four primary turns.

In this setup, noise energy is present at the primary i_{NI} and at the input v_{NI} and output v_{NO} of A_V. As a result, i_{NI} appears in i_L and N_S/N_P and A_V reflect impressions of v_{NO} and v_{NI} to establish a noise current i_N in i_L that is equivalent to

$$i_N = \sqrt{{i_{NI}}^2 + \left[\left(\frac{v_{NI}}{R_P}\right)\left(\frac{N_P}{N_S}\right)\right]^2 + \left[\left(\frac{v_{NO}}{A_V R_P}\right)\left(\frac{N_P}{N_S}\right)\right]^2} \approx i_{NI} . \qquad (6)$$

But since N_S/N_P, R_S, and A_V amplify i_L and i_{NI} in i_S, i_{NI} dominates and v_{NI} and v_{NO}'s impact is low when N_S/N_P is high.

Unfortunately, N_P/N_S also reflects R_P on the primary as R_S or $R_P(N_P/N_S)^2$, which means R_P distorts i_L. This is why i_L's peak in Fig. 6 is lower when N_P is four and the measurement error in Fig. 7 rises with N_P. In other words, fewer turns in the primary reduces noise and improves linearity.

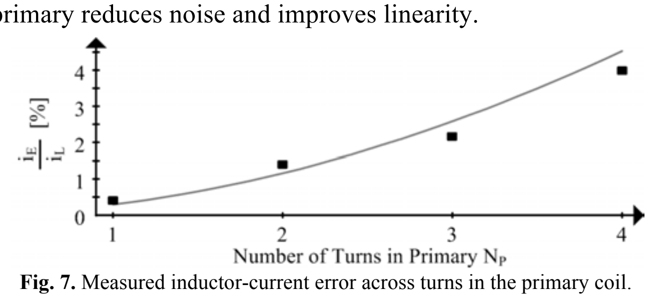

Fig. 7. Measured inductor-current error across turns in the primary coil.

Note L_P only couples L_X's ripple Δi_L to L_S. In other words, i_S cannot monitor i_L's low-frequency components and the effects of A_V's offset v_{OS} are negligible. Although amplifying i_S at low frequency extends this method's effective bandwidth [11], magnetic coupling attenuates i_L at low frequencies so much that v_{NI} overwhelms L_S's impression of i_L in R_P.

IV. SERIES SENSE RESISTOR

Inserting a series resistor R_S [12] like Fig. 8 shows is another way of monitoring i_L. Since R_S distorts i_L, however, R_S must be low, and in consequence, so is R_S's voltage v_S. This is why A_V amplifies v_S in Fig. 8. But since A_V also magnifies input noise $i_{NI}R_S$ and v_{NI}, LPF attenuates frequency components of i_L that are well above the dc–dc converter's switching frequency f_{SW}. This way, dividing LPF's filtered impression of A_V's output by R_S reproduces i_L in i_S, as Fig. 9 demonstrates.

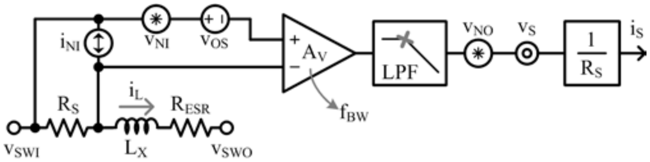

Fig. 8. Series sense-resistor network.

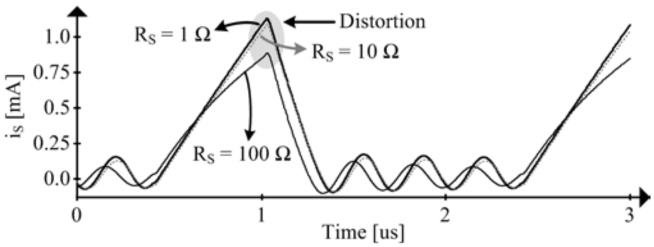

Fig. 9. Measured waveforms for several sense resistances.

Like before, noise current and voltage i_{NI} and v_{NI} are present at A_V's input and noise voltage v_{NO} at A_V's output. As a result, i_{NI} appears in i_L and R_S and A_V reflect impressions of v_{NO} and v_{NI} to establish a noise current i_N in i_L:

$$i_N = \sqrt{{i_{NI}}^2 + \left(\frac{v_{NI}}{R_S}\right)^2 + \left(\frac{v_{NO}}{A_V R_S}\right)^2} \approx \sqrt{{i_{NI}}^2 + \left(\frac{v_{NI}}{R_S}\right)^2}. \qquad (7)$$

But since R_S and A_V amplify i_L, i_{NI}, and v_{NI} in i_S, i_{NI} and v_{NI} dominate and, when R_S and A_V are high, v_{NO}'s impact on i_S in Fig. 10 is low and signal-to-noise ratio SNR in Fig. 11 is high. At some point, though, R_S amplifies i_{NI} to the extent $i_{NI}R_S$ overwhelms v_{NI}, so i_{NI} dominates i_N and i_N becomes insensitive to R_S. This is why SNR flattens at roughly 60 dB when R_S is 60 Ω or higher. In practice, gain A_V and bandwidth f_{BW} in amplifiers are conflicting parameters, so f_{BW} should exceed f_{SW} by 5× or 10×, but not by more for A_V to stay high.

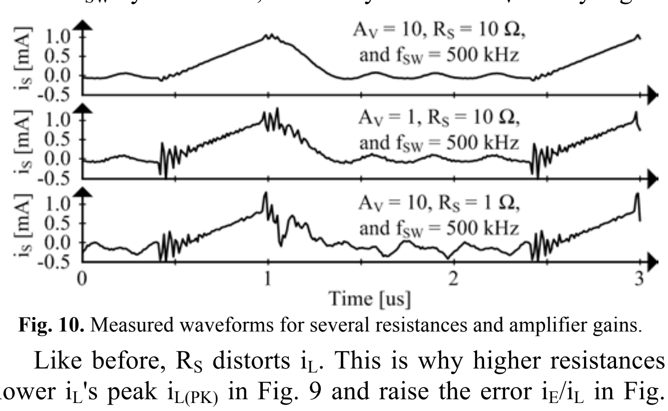

Fig. 10. Measured waveforms for several resistances and amplifier gains.

Like before, R_S distorts i_L. This is why higher resistances lower i_L's peak $i_{L(PK)}$ in Fig. 9 and raise the error i_E/i_L in Fig. 12. In other words, distortion offsets the benefits of lower noise when raising R_S. R_S should therefore be high, but only to the point the error is, for example, less than 5%, which in this case happens at 10 Ω. Note that calibrating the offset that A_V's v_{OS} in Fig. 8 produces in i_S is part of the measurement process.

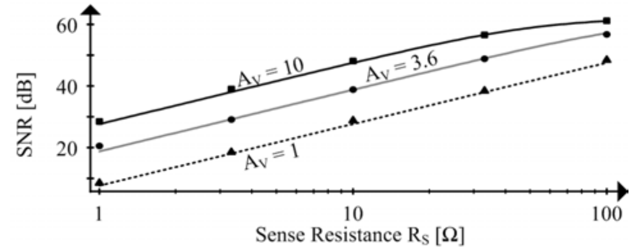

Fig. 11. Measured signal-to-noise ratio across resistances and amplifier gains.

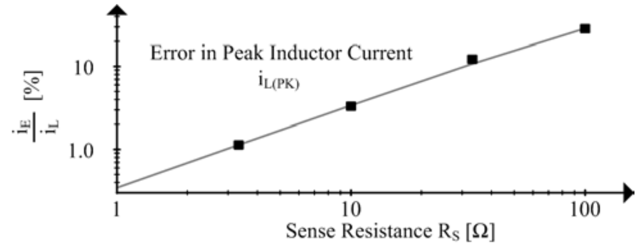

Fig. 12. Measured inductor-current error across sense resistances.

V. CURRENT EXTRACTOR

Another way of measuring i_L is to extract i_L from L_X's terminal voltage v_L [13–14]. Here, the first step is to measure L_X's inductance and series resistance R_{ESR}. With this information, A_V in Fig. 13 can buffer v_L and LPF suppress noise components in A_V's impression of i_L that are well above the system's f_{SW} to produce an observable output v_{OUT}. A computer or a calibrating filter [15] can then divide v_{OUT} by L_X and R_{ESR}'s combined impedance to reproduce i_L in i_S.

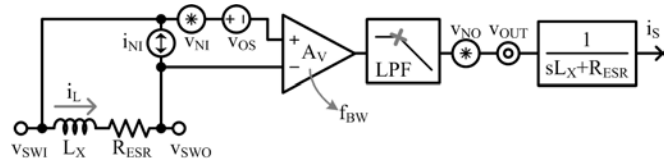

Fig. 13. Inductor-current extractor network.

Thankfully, v_L is in volts, so A_V need not amplify v_L. As a result, A_V's bandwidth f_{BW} can be high. Plus, with a gain of one, A_V no longer amplifies the effects of input noise current and voltage i_{NI} and v_{NI}. And since i_L and i_{NI} drop a higher voltage across L_X and R_{ESR} than they would across R_S, the impact of v_{NI} and v_{NO} on i_L diminishes:

$$i_N = \sqrt{{i_{NI}}^2 + \left(\frac{v_{NI}}{sL_X + R_{ESR}}\right)^2 + \left[\frac{v_{NO}}{A_V\left(sL_X + R_{ESR}\right)}\right]^2}. \qquad (8)$$

In other words, signal-to-noise ratio SNR is nearly 40 dB at 100 kHz in Fig. 14 and about 75 dB at 10 MHz.

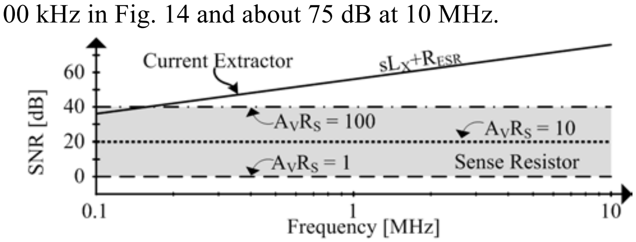

Fig. 14. Measured signal-to-noise ratio across frequency.

Note that integrating v_L across time only indicates how i_L changes with time. In other words, to extract all components of i_L, this method requires i_L's initial value. If this initial value is unknown, i_S and i_L in Fig. 15 differ by an error i_{ERR}:

$$i_{ERR} = i_S - i_L = I_{ERR(I)}\left[1 - e^{-\left(\frac{R_{ESR}}{L_X}\right)t}\right], \quad (9)$$

where $I_{ERR(I)}$ is i_S's initial error. Luckily, i_{ERR} eventually reduces to zero because i_L's average must ultimately match the current that v_L's average establishes across R_{ESR}. This is why i_S is initially off by about 0.5 mA in Fig. 15 and within a few microamps of i_L after 20 µs.

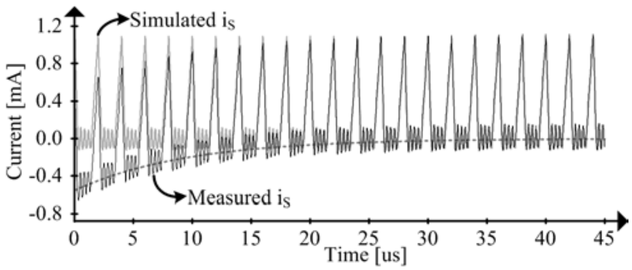

Fig. 15. Extracted inductor current from measured inductor voltage.

VI. Comparison of Measurement Techniques

Of the three methods, as Table I notes, only the coupled probe cannot monitor low-frequency components of the inductor current i_L. And the probe and sense resistor not only amplify input noise but also distort i_L, as Fig. 16 shows. In other words, extracting i_L from measured inductor voltages is more complete, less noisy, and more linear. The only drawback to the extractor is the initial offset that eventually fades.

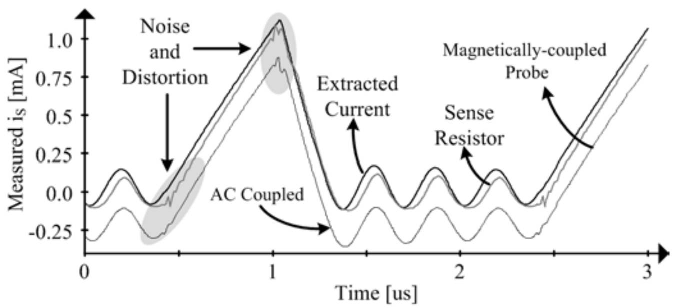

Fig. 16. Measured time-domain currents from all three methods.

Table I: Comparison of Measurement Techniques

	Magnetically Coupled Probe	**Sense Resistor**	**Current Extractor**
Components Monitored	High Frequency	Low and High Frequency	Low and High Frequency
Noise in Measurement	R_P and A_V Amplify Noise	R_S and A_V Amplify Noise	No Amplification
Linearity	Reflected R_P Distorts i_L	R_S Distorts i_L	No Distortion

VII. Conclusions

Measurements show that extracting micro-amp inductor currents in switching dc–dc converters from inductor voltages is more accurate, more linear, and less noisy than monitoring currents with a magnetic probe or a series sense resistor. In fact, distortion is negligible for the extractor and worst-case noise is on par with the resistor's best case in Fig. 14. The importance of these currents is that inductor current determines how well switched-inductor supplies operate. Evaluating this performance is imperative when considering the emerging ubiquity and benefits of wireless microsystems, whose tiny batteries exhaust quickly and supplies resort to switched inductors because they dissipate little power.

Acknowledgment

The authors thank Paul Emerson and Texas Instruments for supporting and sponsoring this research.

References

[1] R. Vullers, *et al.*, "Energy Harvesting for Autonomous Wireless Sensor Networks," *IEEE Solid-State Circuits Magazine*, vol. 2, pp 29-38, 2010.

[2] D. Puccinelli and M. Haenggi, "Wireless Sensor Networks: Applications and Challenges of Ubiquitous Sensing," *IEEE Circuits and Systems Magazine*, vol. 5, pp. 19-31, 2005.

[3] R.D. Prabha, and G.A. Rincon-Mora, "Harvesting Circuits for Minituarized Photovoltaic Cells," *IEEE Int. Symp. on Circuits and Systems,* pp.309-312, May 2011.

[4] K. Cheng, C.Su, and H. Ko, "A High-Accuracy and High-Efficiency On-chip Current Sensing for Current-Mode Control CMOS DC – DC Buck Converter," *Int. Conf. on Electronics, Circuits and Systems,* pp.458-461, Sep 2008.

[5] B. Yuan, and X. Lai, "On-Chip CMOS Current-sensing Circuit for DC-DC Buck Converter," *Electronics Letters*, vol. 45, pp 102-103, Jan 2009.

[6] S. Yuvarajan and L.Wang, "Power Conversion and Control using a current-sensing MOSFET," *Midwest Symposium of Circuits and Systems*, pp. 166-169, May 1991.

[7] J. Chen, *et al.*, "Integrated Current Sensing Circuits Suitable for Step-down DC–DC Converters," *Electroninc Letters*, pp. 200-202, Feb. 2004.

[8] N. Mohan, T. Undeland, and W. Robbins, *Power Electronics Converters, Applications, and Design*, 3rd edn., John Wiley & Sons, Inc., USA, 2003.

[9] H. Kim, M. Falahi T.M. Jahns, and M. Degner, "Inductor Current Measurement and Regulation Using a Single DC Link Current Sensor for Interleaved DC – DC Converters," *IEEE Trans on Power Electronics*, vol. 26, pp. 1503-1510, May 2011.

[10] S. Ang, and A. Olivia, *Power-switching converters, 2nd* edn., Taylor & Francis, USA, 2005.

[11] J. Sanchez-Moreno, *et al.*, "Extending Magnetoresistive AC Transfer Characteristics for Current Measurement," *Instrumentation and Measurement Technology Conf.* pp. 305-308, May 2008.

[12] W. Huang, X. Yang, and C. Ling, "A novel current sensing Circuit for Boost DC – DC Converter," *Anti-counterfeiting, Security and Identification Int. Conf.*, Aug 2012.

[13] A. Simon-Muerla, *et al.*, "Practical Implementation of a High-Frequency Current-Sense Technique for VRM," *IEEE Trans. On Industrial Electronics*, vol. 55, pp. 3221-3230.

[14] C. Chang, "Lossless Current Sensing and Its Application in Current Mode Control," *Power Electronics Specialists Conf.* pp. 4086-4091, June 2008.

[15] H.P. Forghani-zadeh and G.A. Rincon-Mora, "An Accurate, Continuous, and Lossless Self-Learning CMOS Current-Sensing Scheme for Inductor-Based DC – DC Converters," *IEEE J. of Solid-State Circuits*, vol. 42, pp. 665-679, March 2007.